Catalysis Today 163 (2011) 13–19

Contents lists available at ScienceDirect

Catalysis Today

journal homepage: www.elsevier.com/locate/cattod

Synchrotron X-ray microtomography of Raney-type nickel catalysts prepared by gas atomisation: Effect of microstructure on catalytic performance

F. Devred [a,*], G. Reinhart [b], G.N. Iles [b], B. van der Klugt [a], N.J. Adkins [c], J.W. Bakker [a], B.E. Nieuwenhuys [a,d]

[a] Leiden Institute of Chemistry, Leiden University, Einsteinweg 55, 2333 CC Leiden, The Netherlands
[b] ESRF / ILL, Polygone Scientifique Louis Néel, 6 rue Jules Horowitz, 38000 Grenoble, France
[c] CERAM, Queens Road, Penkhull, Stoke-on-Trent, Staffordshire ST4 7LQ, United Kingdom
[d] Eindhoven University of Technology, Schuit Institute of Catalysis, 5600 MB Eindhoven, The Netherlands

ARTICLE INFO

Article history:
Available online 24 February 2010

Keywords:
SXRM
Raney-type nickel catalysts
Gas atomisation process
Leaching process
Nitrobenzene
Butyraldehyde hydrogenation

ABSTRACT

Synchrotron X-ray microtomography (SXRM) was used to examine the microstructure of various Ni–Al alloys prepared by gas atomisation. The resulting Raney-type nickel catalysts that were activated by chemical treatment with a concentrated sodium hydroxide solution (20 wt% in water) were also studied. The main objective of this work is to correlate the microstructure of various Ni–Al alloys prepared by gas atomisation and the catalytic performance of the resulting Raney-type nickel catalysts. It appears that a $NiAl_3/Ni_2Al_3$ ratio around 2.3 in the precursor alloy prepared by gas atomisation favours the formation of a dendritic network in the atomised spherical particle. The spherical shape of the particle and the dendritic network are still present after the leaching process in the Raney-type nickel catalysts. After activation, the interdendritic space forms a macroporous network that is directly linked to the catalytic performance. Parameters of the precursor alloy, i.e. particle size, phase composition, are chosen to obtain an optimal catalytic performance. In this way, an activity is obtained that is at least a factor of 2 higher than that of alloys prepared by the commercial cast-and-crush method. Inductively coupled plasma optical emission spectroscopy (ICP-OES) and BET measurements were used for bulk analysis and determination of the surface area, respectively. Hydrogenation of nitrobenzene and butyraldehyde were used as test reactions. A model that directly correlates the microstructure of a precursor alloy processed by gas atomisation and the catalytic performance of the resulting catalyst is proposed.

1. Introduction

One of the objectives of the IMPRESS Integrated Project [1] is to develop more efficient and cheaper nickel catalyst powders, so-called Raney-type nickel catalysts [2]. Traditionally, aluminium from 50–50 wt% cast-and-crush Ni–Al is leached out by the action of concentrated sodium hydroxide to obtain activated Raney-type nickel catalyst that can be described as an agglomerate of mainly nanoparticles of metallic nickel [3–5]. The activation process determines the structure and properties of the Raney-type nickel catalysts, but the structure and the composition of the starting alloy also play important roles in the performance of the final catalyst [6–9].

In previous work, it was shown that processing by gas atomisation instead of the classical cast-and-crush process to prepare the starting alloy is beneficial in terms of resulting catalytic performance for citral hydrogenation [5]. The amount of $NiAl_3$ present in the starting alloy was found to be crucial in optimising the catalytic performance of the catalyst. The atomisation process appeared to be a key parameter in absolute control of the synthesis of the alloy. A more detailed study that correlates the microstructure of the atomised starting alloy and the microstructure of the resulting catalysts combined with determination of the catalytic performance was then required.

In this paper the catalytic performance of activated atomised alloys with different starting compositions and conventional catalysts prepared by the cast-and-crush process are compared. Synchrotron X-ray microtomography (SXRM) was performed to image the microstructure and the pore structure of the atomised powder before and after leaching. The amount of nickel and remaining aluminium after leaching was determined by elemental analysis using inductively coupled plasma optical emission spectroscopy (ICP-OES). The total surface area of the various catalysts was calculated using BET. Two different reactions were used as test reactions, viz. hydrogenation of nitrobenzene and butyraldehyde.

The aim of this study is to define the parameters for producing a precursor alloy that will lead to optimal catalytic performance. A correlation directly linking the catalytic activity of atomised

* Corresponding author at: Leiden University, Leiden Institute of Chemistry, P.O. Box 9502, 2300 RA Leiden, The Netherlands. Tel.: +31 71 527 4452.
E-mail addresses: F.Devred@chem.leidenuniv.nl, fdevred@yahoo.fr (F. Devred).

0920-5861/$ – see front matter © 2010 Elsevier B.V. All rights reserved.
doi:10.1016/j.cattod.2010.01.054

Raney-type nickel catalysts to the precursor alloy synthesis is described.

2. Experimental

2.1. Alloy preparation

Within the IMPRESS project, in parallel to the conventional cast-and-crush process to prepare the nickel aluminium alloy, another production process is currently being investigated to achieve improvements in Ni–Al powders: gas atomisation. This process has been described in previous work [5,10]. Compared to the conventional cast-and-crush technique, it can produce fine, clean and spherical particles. Atomised powders are prepared at CERAM (UK). Raney-type catalysts are usually prepared from 50–50 wt% (31.5–68.5 at%) Ni–Al alloys. It was demonstrated in a previous paper that the amount of $NiAl_3$ in the starting atomised alloy is a key parameter to optimise the catalytic performance [5]. Several Ni–Al atomised alloys with various compositions were prepared (68.5 at% Al, 72 at% Al, 75 at% Al, 77.5 at% Al, 78.75 at% Al, 80 at% Al and 82.5 at% Al). The powders were sieved and two different ranges of particle sizes were retained for analysis: 75–106 and 106–150 μm. For comparison, cast-and-crush powders from ACCESS (DE) were also investigated (68.5 at% Al and 75 at% Al, 40–90 and 90–180 μm).

2.2. Sequential leaching

Starting powders were treated with an excess of aqueous 20 wt% sodium hydroxide solution according to the following equation:

$$2(Ni{-}Al)_{(s)} + 2OH_{(aq)}^{-} + 6H_2O_{(l)} \rightarrow 2Ni_{(s)} + 2Al(OH)_{4(aq)}^{-} + 3H_{2(g)}\,[11].$$

An excess of concentrated sodium hydroxide (more than 10 wt%) is required to avoid the precipitation of Bayerite ($Al_2O_3{\cdot}H_2O$), which can block the pores of the catalyst by covering the nickel surface [11]. The powder was slowly introduced into the sodium hydroxide solution (20 wt%) at 50 °C. Due to the exothermic reaction, the temperature increased quickly to around 80 °C, which was kept constant during the reaction. After 180 min reaction time, no further evolution of H_2 was observed for various binary precursor alloys, meaning that the accessible amount of Al had been completely transformed to a hydroxide state that dissolved into the sodium hydroxide solution. The sodium hydroxide solution was then removed and the resulting powders were washed in distilled water. To avoid exposure to air, different samples were kept immersed in water prior to the characterisation experiments.

2.3. Characterisation techniques

2.3.1. ICP-OES

Elemental analysis was performed by ICP-OES (inductively coupled plasma optical emission spectroscopy) using a Varian Vista-MPX spectrometer. For that purpose, around 0.05 g of powder was dissolved in a 6% solution of nitric acid and the solution was diluted by a factor of 1000 with distilled water before measurement.

2.3.2. Synchrotron X-ray microtomography

Microtomography experiments were carried out on powders before and after leaching at the ID19 beamline of the European Synchrotron Radiation Facility (ESRF) [12] within the framework of the ESA-ESRF-ILL collaboration [13]. Atomised alloy particles that consist of spherical grains of 75–106 μm were encapsulated into capillaries of 350 μm inner diameter. This corresponds to the chosen field of view when using a 2048 × 2048 FReLoN camera and an optic allowing a pixel resolution of 0.17 μm/pixels. Usual storage in a solvent like water was not feasible during the acquisition of pictures due to the formation of bubbles when the sample was exposed to X-rays which would prevent exploitation of the collected data. Powders after leaching were thus passivated resulting in the formation of a thin oxide layer. The passivation process was performed by placing the damp powder into a vacuum desiccator. The powder was dried by evacuating the desiccator for 4 h. Air was then slowly introduced into the desiccator through a fine hypodermic needle (48 h to atmospheric pressure). The energy was set to 20.5 keV in order to optimise the X-ray flux and the contrast between the different phases present in the grains.

2.3.3. BET measurements

BET surface areas of the catalysts were measured by N_2 physisorption at −196 °C with an automatic Qsurf M1 analyzer (Thermo Finnigan). A special cell was designed to dry the Raney-type nickel catalysts by evacuating the liquid. Then, before each measurement the catalyst was degassed for 3 h in helium at 150 °C to remove the adsorbed impurities. For each measurement at least three points were taken into account to calculate the total surface area of the samples.

2.4. Hydrogenation reactions

The hydrogenation experiments were performed in a 100 ml batch autoclave manufactured by Parr Industry using a working pressure of 4.0 MPa and 40 °C. The reactor was first purged with H_2 at room temperature. For both hydrogenation reactions, 0.3 g of wet catalyst and 5 ml of reactant were introduced with the solvent (60 ml of methanol for nitrobenzene hydrogenation and 60 ml of 1-propanol for butyraldehyde hydrogenation). The liquid/gas ratio in the reactor was about 2/3 in both cases. When the preset temperature was reached, the hydrogen pressure was set to the desired pressure and stirring of the mixture was started. The concentrations of the reactant and the reaction products were followed by gas chromatography using a HP 5890 GC equipped with a SGE forte GC capillary column. Helium was used as carrier gas. The column temperature was kept at a constant temperature of 110 °C (nitrobenzene hydrogenation) and 50 °C (butyraldehyde hydrogenation). The gas chromatograph was directly coupled to the reactor to allow on-line experiments. The concentration of the components was calculated based on the peak areas. From the data, a concentration profile was plotted (percentage of reactant and products versus time). From this concentration profile, the activity was calculated from the decrease in reactant concentration in the linear range between 20% and 80% conversion and was expressed in mol $kg_{cat}^{-1} min^{-1}$ at 50% conversion. A test on mass transfer limitations showed that the reaction rate is independent of the stirring rate at speeds above 1000 rpm.

3. Results and discussion

3.1. Synchrotron X-ray microtomography

SXRM techniques can be used to characterise macroporous materials (pore width >1 μm) [14] and especially heterogeneous catalysts [15]. Nevertheless, to our knowledge, no SXRM studies of Raney-type nickel catalysts have been performed so far. The image analysis (phase/density contrasts) of radiographs collected at different angles generates the phase composition of the precursor alloy whereas the 3D reconstruction of the 2D cross sections radiographs allows visualisation of the pore structure.

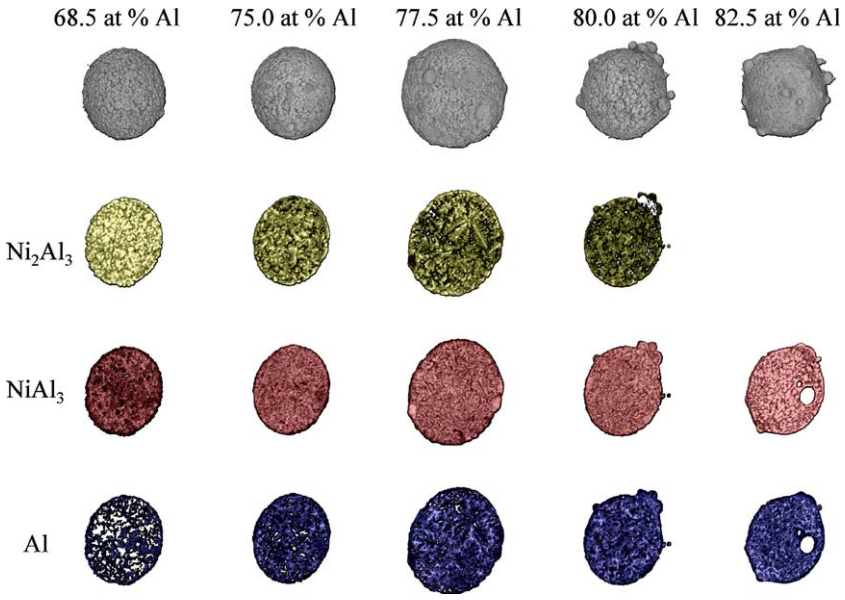

Fig. 1. Synchrotron X-ray microtomography: 3D reconstruction of atomised grain (top line), visualisation of the microstructure of the three different phases.

3.1.1. Precursor atomised alloy

In the range of compositions of interest, Ni–Al alloys that are used to prepare Raney-type nickel catalysts contain three different main phases: Ni_2Al_3, $NiAl_3$ and metallic Al that comes from the eutectic $NiAl_3$–Al [3,5]. $NiAl_3$ and the eutectic react easily with sodium hydroxide solution whereas the aluminium contained in the Ni_2Al_3 phase is much more difficult to leach out. Bakker et al. [16] found that the leaching kinetics are approximately linear in the case of the $NiAl_3$ phase, while for Ni_2Al_3, the kinetics are parabolic. Due to a higher cooling rate in comparison to the classical cast-and-crush process, the atomisation process might lead to some deviation in the equilibrium phase compositions that then affect the catalytic performance of the resulting catalysts. The microstructures of five atomised precursor alloy particles with various compositions were reconstructed by SXRM. In Fig. 1, a cross section of a particle of each atomised powder shows qualitatively the phase distribution of the three main phases as a function of the initial composition. The Ni_2Al_3 phase is the first to solidify, then $NiAl_3$ and finally some eutectic Al-$NiAl_3$. In comparison to the Ni–68.5 at% Al, formation of a dendritic network is clearly visible for the Ni–75 at% Al and especially for Ni–77.5 at%. The presence of dendrites appears to be a major difference regarding the microstructure in comparison with classical cast-and-crush particles in which the phase distribution was described as a kernel of Ni_2Al_3 with an outer shell of $NiAl_3$ [3]. Within the IMPRESS project, high resolution transmission electron microscope (HRTEM) studies were performed to fully understand the dendritic microstructure of the atomised powders [17]. It appears that the backbones of the dendrites mainly contain Ni_2Al_3 and are covered with $NiAl_3$. The interdendritic space formed by the dendritic network is then filled with the aluminium coming from the Al–$NiAl_3$ eutectic. Those results are in good agreement with what is observed by SXRM. No Ni_2Al_3 is present in the Ni–82.5 at% Al. A 'spherical hole' is visible in the microstructure, due to a trapped bubble of argon during the atomisation process.

The phase compositions were also determined. In Fig. 2, the evolution of the phase content is plotted as a function of the starting elemental composition of the atomised alloys. As expected, the more aluminium there is in the starting alloy, the less Ni_2Al_3 in the starting alloy. Those results are in excellent agreement with neutron diffraction experiments [18] that were performed within the IMPRESS project on the same samples.

3.1.2. Leached catalysts

After activation (leaching process), three catalysts prepared from atomised alloys with different compositions (Ni–68.5 at% Al, Ni–75 at% Al and Ni–82.5 at%) were studied. In Fig. 3, the 3D reconstruction of the grain and a cross section for each composition are represented to visualise the microstructure after leaching. In this figure, the Raney-type nickel catalyst that consists mainly of Ni is represented in grey while the micropores of the catalysts are represented in blue. (For interpretation of the references to colour in this figure legend, the reader is referred to the web version of this article.) The first important result that was already described in a previous publication [5] is the confirmation that the original size of the grain (around 80 μm) is conserved despite the leaching process. This is of real interest since the particle size of the catalysts can be selected directly by the atomisation process followed by a

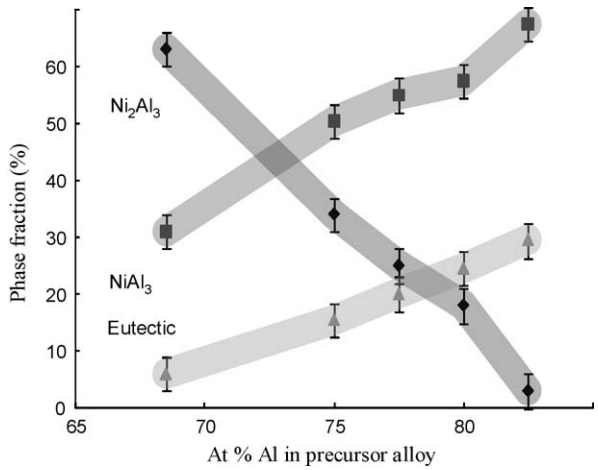

Fig. 2. Quantitative analysis: phase fraction as a function of aluminium content in the atomised alloy.

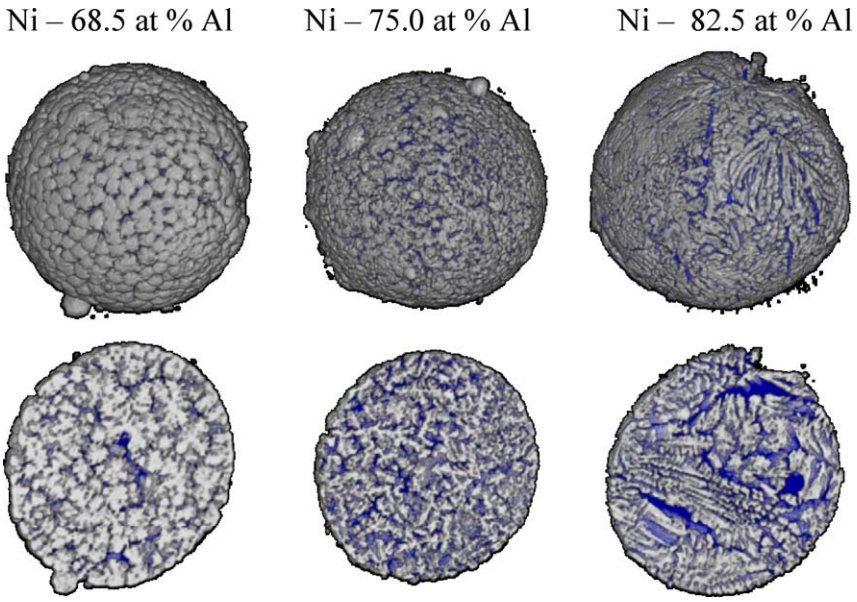

Fig. 3. Synchrotron X-ray microtomography: 3D reconstruction and cross section of activated catalysts prepared from the atomised alloy.

sieving process before activation of the catalyst. As for the starting alloy, a fine dendritic network is visible in the activated catalyst prepared from Ni–75 at% Al. We can assume that the backbone of the dendritic structure remains intact after the leaching process. This is in excellent agreement with the work of Hormann et al. [17] that described within the IMPRESS project the microstructure of the catalyst prepared from an atomised alloy and studied by HRTEM. They reported that after activation, the backbones of the dendrites consist of a dense phase that still contains a significant amount of aluminium (up to 20 at%) originating from the Ni_2Al_3 phase. The backbones are covered by capping layers that consist of almost pure nickel. A mesoporous network was observed by TEM in the structure of the capping layers [17], which cannot be seen by SXRM. The macroporous network that forms during the leaching process might be due to the dissolution of the eutectic phase. This macroporous network is represented in blue in Fig. 3.

A 3D reconstruction of the particle is computed to encompass the activated catalyst within a defined volume. Each volume unit (voxel) can be attributed either to the bulk structure of the catalyst or to its surface. Image processing is used to generate a volume (mask) including both the voxels related to the bulk structure and the inner void. Voxels obtained by performing the difference between the mask and the bulk structure are then attributed to the "void" formed by the macroporous network.

Quantitative relative numbers can then be defined:

- (voxels at the surface/volume of the bulk structure) defines the normalised specific surface of the macroporous network.
- [(volume of the mask – volume of structure)/volume of the mask] defines the normalised volume of void (porosity).

The results are shown in Fig. 4. A clear trend correlating the starting composition of the atomised alloy to the microstructure of the resulting catalyst is illustrated. As already mentioned, increasing the amount of aluminium in the starting alloy (75 at% Al) favours the solidification of Ni_2Al_3 as fine dendrites. After the activation process, the dendritic structure of the original Ni_2Al_3 phase remains and favours the formation of a macroporous network. By comparing the catalysts prepared from the 68.5 at% alloy and the 75 at% alloy, significant increases in the porosity (micropores) and the surface area of the catalysts were observed. If no Ni_2Al_3 is present in the starting alloy (82.5 at% alloy), one can assume that the dendritic network due to the Ni_2Al_3 phase is barely formed and therefore, the surface area

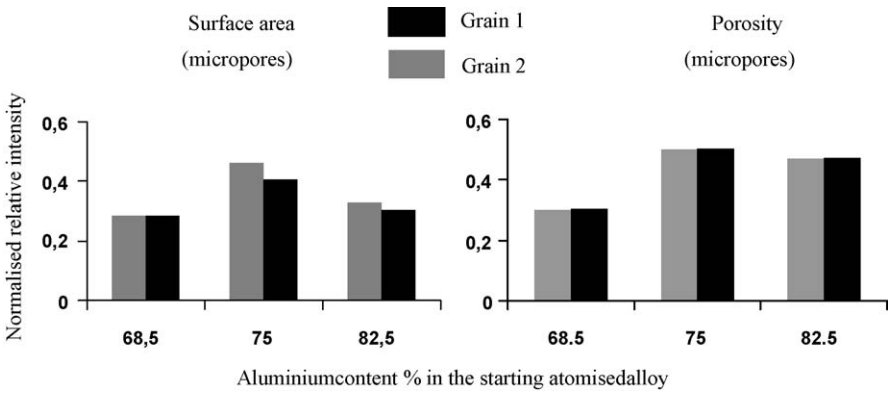

Fig. 4. Quantitative analysis: synchrotron X-ray microtomography on activated atomised catalysts.

Table 1
ICP-OES and BET data.

Original alloy	Original grain size	at% Ni (bulk)	BET ($m^2 g^{-1}$)
Atomised			
Ni–68.5 at% Al	75–106 μm	68	56
Ni–68.5 at% Al	106–150 μm	67	61
Ni–72.5 at% Al	75–106 μm	74	53
Ni–72.5 at% Al	106–150 μm	73	58
Ni–75 at% Al	75–106 μm	83	52
Ni–75 at% Al	106–150 μm	83	55
Ni–77.5 at% Al	75–106 μm	84	63
Ni–77.5 at% Al	106–150 μm	84	58
Ni–78.75 at% Al	75–106 μm	84	62
Ni–78.75 at% Al	106–150 μm	84	59
Ni–80 at% Al	75–106 μm	86	48
Ni–80 at% Al	106–150 μm	86	49
Ni–82.5 at% Al	75–106 μm	89	48
Ni–82.5 at% Al	106–150 μm	90	50
Cast-and-crush			
Ni–68.5 at% Al	40–90 μm	70	58
Ni–68.5 at% Al	90–180 μm	72	63
Ni–75 at% Al	40–90 μm	76	55
Ni–75 at% Al	90–180 μm	77	62

and the porosity (micropores) of the resulting catalysts would be negatively affected.

It can be concluded that there is an ideal $NiAl_3/Ni_2Al_3$ ratio in the original alloy exists that would generate a dendritic structure in which microporosity and surface area of that macroporous network are optimum.

3.2. BET surface area and elemental analysis (ICP-OES) of activated samples

Results of bulk (ICP-OES) and BET measurements are reported in Table 1. For each starting alloy, two different ranges of particle sizes were studied. No significant differences were observed between catalysts prepared from alloys with the same starting composition but different particle size. BET measurements give the total surface area of the catalysts. The total surface area is found to be similar for all the samples studied, and, therefore, the difference in catalytic activity cannot be explained in terms of the difference in surface area. It is important to note that, in comparison to the SXRM technique, the BET measurement technique also measures the surface area of the mesopores (5–10 nm [17]). In the present work, one can assume that the surface area of the macroporous network estimated by SXRM is not significant in comparison to the BET surface area that reaches values around 50–60 $m^2 g^{-1}$. No significant differences in BET surface area were observed between the various catalysts, and the trend observed in catalytic performance is the same if expressed per gram of catalyst or per surface of catalyst.

Another interesting result is the difference in measured bulk concentration between the samples: the more aluminium in the precursor alloy, the less remaining aluminium in the final catalyst. This result is expected as increasing the aluminium content in the alloy will also decrease the concentration of Ni_2Al_3, the most difficult phase to leach. This result is more pronounced in the case of atomised samples than cast-and-crush samples. In the 68.5 at% samples for cast-and-crush and atomisation processes, around 30 at% Al remains. In the 75 at% samples, around 17 at% Al remains in the case of atomisation process whereas 23–24 at% Al remains for the cast-and-crush samples. This difference can be explained by the creation of the macroporous network and the dendritic structure for atomised alloys favouring the action of the sodium hydroxide solution.

3.3. Hydrogenation reactions and catalytic performance

3.3.1. Butyraldehyde and nitrobenzene hydrogenations

Nitrobenzene is mainly produced as a precursor to aniline. Aniline is the simplest and most important aromatic amine, being used as an intermediate in the production of more complex chemicals. Its main application is in the manufacture of polyurethane; it is also used for production of pharmaceuticals, explosives or agricultural products [19,20]. A simplified reaction scheme and a typical concentration profile of nitrobenzene hydrogenation are presented in Fig. 5. Various intermediate products might form along with the desired product: aniline. Those are nitrosobenzene and phenylhydroxylamine but also undesired products due to a dimerisation process: azoxybenzene, azobenzene and hydrazobenzene (not shown in Fig. 5) [21,22]. Under our experimental conditions, only nitrosobenzene is observed as an intermediate

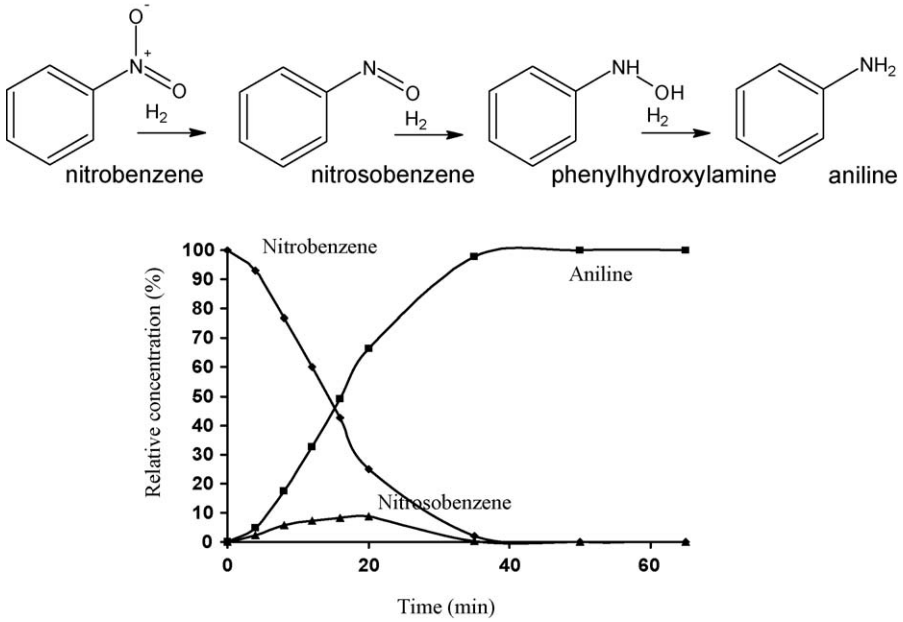

Fig. 5. Reaction scheme and typical concentration profile of the nitrobenzene hydrogenation reaction.

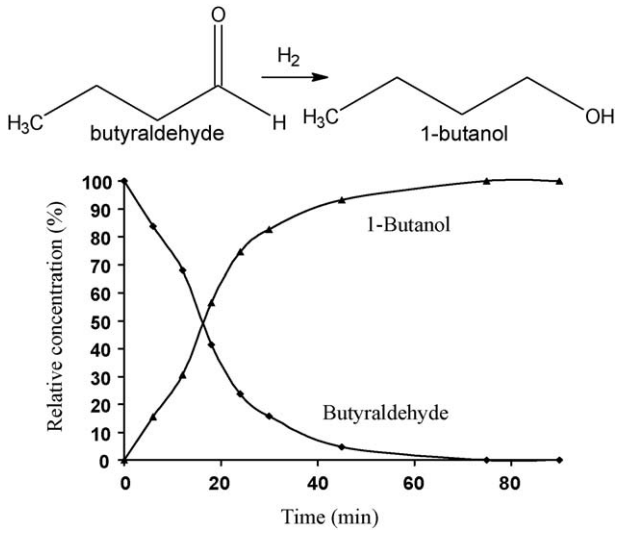

Fig. 6. Reaction scheme and typical concentration profile of the butyraldehyde hydrogenation reaction.

product in a quantity never higher than 10%. The hydrogenation reaction occurs through the direct pathway, i.e. without formation of azoxybenzene, azobenzene or hydrazobenzene. The hydrogenation of nitrobenzene to nitrosobenzene is the rate determining step. For each catalyst tested, 100% of aniline was obtained after less than 100 min of reaction time.

Butyraldehyde is used in the synthesis of butanol, which is mainly used as a solvent, an intermediate in chemical synthesis or as a fuel [23]. The simplified reaction schemes and the concentration profiles of butyraldehyde hydrogenation are presented in Fig. 6. Under our experimental conditions butyraldehyde is fully converted into 1-butanol. Butyric acid, formed when butyraldehyde is exposed to air, was not observed. Both hydrogenation reactions are ideal reaction tests with which to compare the catalytic activity (initial reaction rate) of the various studied catalysts.

3.3.2. Catalytic performance

The catalytic activities of the catalysts prepared from atomised and cast-and-crush alloys with various compositions are shown in Fig. 7 for both hydrogenation reactions. In the case of catalysts prepared by atomisation, an optimal activity is observed for the catalyst prepared from the Ni–77.5 at% Al alloy for both nitrobenzene and butyraldehyde hydrogenation. Increasing the amount of aluminium (which also means increasing the amount of the $NiAl_3$ phase) has a positive effect on catalytic activity up to 77.5 at% Al.

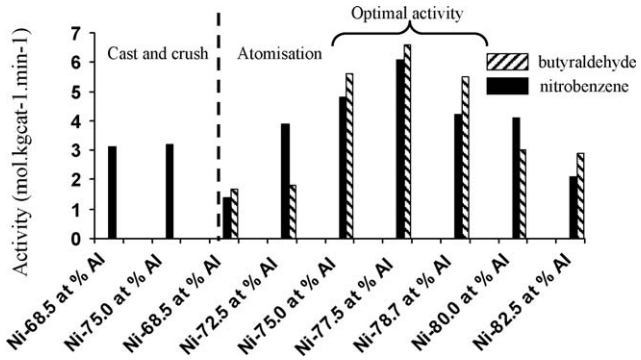

Fig. 7. Catalytic activities (nitrobenzene and butyraldehyde hydrogenations) of catalysts prepared from precursor alloys with various compositions (atomisation and cast-and-crush processes).

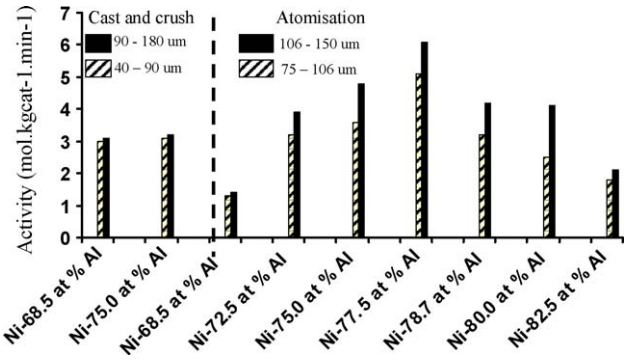

Fig. 8. Nitrobenzene hydrogenation: catalytic activity, particle size and precursor alloy compositions.

Adding extra aluminium results in a lower activity. The catalyst prepared from the 68.5 at% Al cast-and-crush alloy shows a much higher activity than the catalyst prepared from the atomisation process with the same composition. However, increasing the amount of aluminium in the cast-and-crush catalysts has no effect on the resulting catalytic activity (nitrobenzene hydrogenation). The optimal starting composition for the alloy window is now defined: 77.5 at% Al in the atomised alloy, corresponding to a $NiAl_3/Ni_2Al_3$ ratio of about 2.3, exhibits the highest catalytic activity.

In the case of nitrobenzene hydrogenation the influence of the particle size was studied. For each starting composition two different ranges of particle size were compared (75–106 and 106–150 μm for atomisation process, 40–90 and 90–180 μm for the cast-and-crush process). The results are shown in Fig. 8. No particle size effect was observed in the case of catalysts prepared by cast-and-crush process. For the atomisation samples, the 106–150 μm series was slightly better in terms of activity than the 75–106 series irrespective of the starting compositions. The trend for both series remains identical: the Ni–77.5 at% Al atomised alloy leads to the most active catalyst after activation.

3.3.3. Relationship of microstructure–catalytic activity

Extra information can now be added to the model we proposed previously [5]. In this model, based on studies using citral hydrogenation, it was suggested that increasing the amount of $NiAl_3$ in the atomised starting alloy also increases the activity. What was only speculation is now confirmed. However, this model is only valid for a certain range of compositions of the starting material as the presence of Ni_2Al_3 phase is necessary to form the spongy structure during leaching [16,24]. Increasing the volume fraction of the $NiAl_3$ phase in the starting alloy too much prevents the formation of the macroporous and dendritic structure that remains after leaching and leads to a decrease in catalytic performance. Optimal parameters (phase composition, phase ratio and particle size) have to be defined in order to obtain an optimum macroporous network in terms of micropore volume and the available surface area due to those micropores. The slight particle size effect observed in terms of catalytic activity may suggest that the formation of the optimum macroporous network requires relatively large grains of atomised powders. In the case of the cast-and-crush process, no significant difference in activity was observed between catalysts prepared from two different phase compositions and two different particle sizes. It emphasises the importance of the formation of the dendritic structure that is observed only in the case of atomisation process. In our previous work [5], the best catalytic activity was described to be dependent on the aluminium content in the final catalyst: the less aluminium in the final catalyst, the better the activity. This argument remains

true within a defined working window. For instance, less aluminium will remain in the atomised Ni–82.5 at% Al catalyst but its catalytic activity will be poor because of the absence of Ni_2Al_3 phase that ensures the formation of the dendritic network.

4. Conclusions

In this work, optimal parameters have been defined to design the best activity of a Raney-type nickel catalyst for the hydrogenation of nitrobenzene and butyraldehyde:

- Atomisation process.
- $NiAl_3/Ni_2Al_3$ ratio in the precursor alloy = 2.3.
- Grain size in the precursor alloy from 106 to 150 μm.

Regarding the experimental conditions for the atomisation process and the hydrogenation reactions, these parameters lead to an optimum Raney-type nickel catalyst. Using the atomisation process instead of the classical cast-and-crush process favours the solidification of the Ni_2Al_3 phase as a fine dendritic structure. This structure remains in the catalysts after the activation process and a macroporous network is then created in the interdendritic space. One can speculate that the interdendritic space was mostly filled with the eutectic Al-$NiAl_3$ as the easiest phase to dissolve during the activation process. The choices of the right $NiAl_3/Ni_2Al_3$ ratio and the right range of grain size favour an optimal macroporous structure in terms of volume of micropores (porosity) and subsequently, surface available due to those micropores. The catalytic activity if the proper parameters were chosen was two times higher than that for a catalyst produced by the classical industrial cast-and-crush process. The remarkable result is that the parameters defined previously concerned only the preparation of the precursor alloy. A direct link has therefore been established between catalytic activity and microstructure of the precursor alloy particles.

Acknowledgements

This work is part of the EU IMPRESS project (Intermetallic Materials Processing in Relation to Earth and Space Solidification) [1]. The authors would like to express their gratitude for financial support from IMPRESS Integrated Project (Contract NMP3-CT-2004-500635) co-funded by the European Commission in the Sixth Framework Programme and the European Space Agency. The authors would also like to thank Elodie Boller and Paul Tafforeau from the ESRF for their useful technical support in processing the microtomography data.

References

[1] D.J. Jarvis, D. Voss, Mater. Sci. Eng. A 413–414 (2005) 583.
[2] M. Raney, US Patent 1,563,787 (1925).
[3] F. Devred, B.W. Hoffer, W.G. Sloof, P.J. Kooyman, A.D. van Langeveld, H.W. Zandbergen, Appl. Catal. A: Gen. 244 (2) (2003) 291.
[4] J. Rothe, J. Hormes, C. Schild, B. Pennemann, J. Catal. 191 (2000) 294.
[5] F. Devred, A.H. Gieske, N. Adkins, U. Dahlborg, C.M. Bao, M. Calvo-Dahlborg, J.W. Bakker, B.E. Nieuwenhuys, Appl. Catal. A: Gen. 356 (2009) 154.
[6] A.B. Fasman, V.F. Timofeeva, V.N. Rechkin, Y.F. Klyuchnikov, Kyn. Khem. 13 (1971) 1513.
[7] J Freel, W.J.M. Pieters, R.B. Anderson, J. Catal. 14 (1969) 247.
[8] S. Sane, J.M. Bonnier, J.P. Damon, J. Masson, Appl. Catal. 9 (1984) 69.
[9] M.S. Wainwright, in: G. Ertl, H. Knozinger, J. Weitkamp (Eds.), Handbook of Heterogeneous Catalysis, vol. 1, VCH Publ., New York, 1997,ISBN 3-527r-r29212-8.
[10] M. Tong, D. Browne, J. Mater. Process. Technol. 202 (1–3) (2008) 419.
[11] P. Fouilloux, Appl. Catal. 8 (1983) 1.
[12] G. Reinhart, G.N. Iles, C.-A. Gandin, D. Tourret, F. Devred, H. Henein, M. Calvo-Dahlborg, U. Dahlborg, E. Boller, ESRF Experimental Report MA-636, 2009.
[13] G. Reinhart, G.N. Iles, G.J. McIntyre, A.N. Fitch, D.J. Jarvis, Mater. Res. Soc. Symp. Proc. 1128-U03-11 (2009).
[14] S. Blacher, V. Maquet, A. Léonard, G. Chapelle, M. Crine, R. Jérome, J.-P. Pirard, Stud. Surf. Sci. Catal. 144 (2002) 331.
[15] K.W. Jones, P. Spanne, S.W. Webb, W.C. Connor, R.A. Bayerlein, W.J. Reagan, F.M. Dautzenberg, Nucl. Instrum. Methods Phys. Res. B56/57 (1991) 427.
[16] M.L. Bakker, D.J. Young, M.S. Wainwright, J. Mater. Sci. 23 (1988) 3921.
[17] U. Hörmann, U. Kaiser, N. Adkins, R. Wunderlich, A. Minkow, H. Fecht, H. Schils, T. Scherer, H. Blumtritt, EMC, 2008, 14th European Microscopy Congress 1-5 September 2008, Aachen, Germany. S. Richter, A. Schwedt (Ed.), Springer (2008) 217.
[18] C.M. Bao, U. Dahlborg, N. Adkins, M. Calvo-Dahlborg, J. Alloys Compd. 481 (1–2) (2009) 199.
[19] X. Meng, H. Cheng, Y. Akiyama, Y. Hao, W. Qiao, Y. Yu, F. Zhao, S. Fujita, M. Arai, J. Catal. 264 (2009) 1.
[20] A.S. Travis, in: Z. Rappoport (Ed.), The Chemistry of Anilines, John Wiley and Sons, 2007, p. 715.
[21] F. Cardenas-Lizana, S. Gomez-Quero, M.A. Keane, Appl. Catal. A 222 (2008) 199.
[22] P. Baumeister, H.U. Blaser, M. Studer, Catal. Lett. 49 (1997) 219.
[23] H. Noller, W.M. Lin, J. Catal. 85 (1984) 25.
[24] A.J. Smith, D.L. Trimm, Annu. Rev. Mater. Res. 35 (2005) 127.